Hierarchical MIMO Decoupling Control for Vehicle Roll and Planar Motions With Control Allocation

Fengchen Wang, *Member, IEEE*, Yue Shi, and Yan Chen, *Member, IEEE*

***Abstract*—Although many methods of ground vehicle dynamics control have been widely studied, their robustness against undesirable oscillatory coupling behaviors of planar and roll dynamics is not fully explored. To address this issue, a hierarchical multiple-input-multiple-output (MIMO) decoupling controller is proposed in this study. Based on the hierarchical control configuration, the coupled vehicle roll and planar dynamics are resolved in the high-level control, and a control allocation is utilized for tracking control in the low-level control. The decoupled internal dynamics and nominal stability are then analyzed and proved. Moreover, by using the vehicle yaw rate and load transfer ratio, a control trigger with dynamic weighting is designed to guarantee the feasibility of the MIMO decoupling control and smooth control efforts. Through the co-simulation between CarSim and MATLAB/Simulink, the feasibility and effectiveness of the proposed controller are verified.**

***Index Terms*—Decoupling control, feedback linearization, stabilization, rollover, vehicle dynamics.**

I. Introduction

RECENTLY, the thriving market of the automotive industry promotes the explosion of new vehicle electrification and automation technologies, such as steer-by-wire actuation systems and distributed propulsion architectures with in-wheel motors (IWMs) [1], [2]. One significant advantage of vehicle electrification and automation is to provide over-actuated features with redundant actuators, which can further improve vehicle safety, energy efficiency, and agility through sophisticated control design. For instance, the energy efficiency improvement for electric vehicles with four IMWs in both longitudinal and lateral motions was investigated via different optimal control and torque distribution methods [3], [4], [5], [6].

For safety improvement, the stability control of over-actuated vehicles was studied in the literature [7], [8]. The authors studied vehicle lateral stability enhancement through a hierarchical over-actuated control scheme based on an active yaw stabilizer [7], and roll stability enhancement through the integration of an active rollover preventer and active front steering control [8], respectively. Generally, vehicle lateral/yaw and roll motions are controlled independently based on the assumption that vehicle lateral/yaw instability and rollover usually happen on different driving scenarios [9]. Hence, the control mode switching method could be employed, in which the mode of vehicle dynamics control is determined by rollover indexes [10]. Namely, once the threshold of a rollover index is reached, the control objective is switched from vehicle lateral/yaw stabilization to rollover prevention. However, during some aggressive driving maneuvers, vehicle lateral/yaw stability and rollover prevention must be simultaneously considered, even if their control objectives may be conflicting.

To balance and compromise the conflicting control objectives, one way is to take the advantages of over-actuated vehicle systems. For instance, a hierarchical control framework with control allocation (CA) was introduced in [11] to resolve the conflicting issue explicitly. In a hierarchical configuration, the virtual control inputs in the high level ensured vehicle lateral/yaw stability, and the optimal control allocation problem in the low level was designed to mitigate the rollover propensity [11]. In [12] and [13], model predictive control (MPC) was used to keep vehicle lateral/yaw stable and minimize the rollover indexes simultaneously.

Although the CA and MPC methods can deal with vehicle lateral/yaw and roll dynamics control together by resolving optimization problems, the unexpected nonlinear coupling behaviors of planar (i.e., longitudinal, lateral, and yaw) and roll dynamics are not fully explored. Vehicle lateral/yaw and roll dynamics were considered separately in cost functions and constraints in the optimization problems [11]. As a result, the dynamic coupling components between vehicle lateral/yaw and roll dynamics were usually ignored [11], [12], [13]. In addition, the coupling dynamics cannot be directly handled in either cost functions or constraints, which will be illustrated in Section II. On the other hand, the impacts of nonlinear coupling dynamics can make vehicle states oscillatory or even unstable due to common vehicle disturbances and uncertainties, such as side wind, road unevenness, and cargo load variations [14]. Thus, it is essential to investigate the coupling dynamics for vehicle stability control.

In nonlinear control theory, feedback linearization and input-output decoupling control are usually employed to handle the coupling issues of nonlinear dynamics. The corresponding applications on vehicle planar dynamics control were reported [15], [16], [17]. For example, an asymptotic decoupling control was studied for sideslip angle and yaw rate to provide the desired linear vehicle dynamics of outputs regardless of disturbances [16]. A decoupled four-wheel steering (4WS) control was

Manuscript received 21 September 2022; revised 2 March 2023 and 28 June 2023; accepted 19 August 2023. Date of publication 25 August 2023; date of current version 17 January 2024. The review of this article was coordinated by Dr. Chuan Hu. *(Corresponding author: Yan Chen.)*

Fengchen Wang is with the College of Computing, Georgia Institute of Technology, Atlanta, GA 30332 USA (e-mail: felixw@gatech.edu).

Yue Shi and Yan Chen are with the Polytechnic School, Arizona State University, Tempe, AZ 85212 USA (e-mail: yueshi@asu.edu; yanchen@asu.edu).

Digital Object Identifier 10.1109/TVT.2023.3308577

investigated to consider varying longitudinal speeds [17]. Inspired by the decoupling control of vehicle planar motions, the idea of input-output decoupling can be extended to stabilize vehicle planar and roll dynamics simultaneously.

Motivated by the aforementioned coupling issues between the vehicle planar and roll dynamics, the authors proposed a hierarchical input-output decoupling (HIOD) controller with control allocation by integrating 4WS control and four-IWMs independent driving/braking control in [18]. The HIOD controller can prevent vehicle rollover as well as keep the input-output lateral/yaw $\mathcal{L}_\infty$ stability of the vehicle planar motion. Nevertheless, the chattering issue occurred in control efforts, and the small-signal finite-gain $\mathcal{L}_\infty$ stability may not be fast enough to stabilize vehicles in motion. Therefore, to extend the authors' previous work [18], this article has three additional contributions involving multi-input multi-output (MIMO) decoupling methods as follows.

1) A MIMO decoupling matrix is established to decouple nonlinear vehicle dynamics after introducing feedback linearization for vehicle roll dynamics. Using the decoupling matrix, the input-output vehicle model can be decoupled and stabilized by the derived input-output decoupling control law.
2) A hierarchical MIMO decoupling (HMMD) control with control allocation is proposed. A dynamic control trigger is also designed to guarantee the feasibility of the MIMO decoupling control and generate smooth control efforts without frequently turning the controller on and off.
3) The decoupled internal dynamics and nominal exponential stability are also analyzed, which is better than the $\mathcal{L}_\infty$ stability with a faster convergence speed. The co-simulation integrating CarSim and MATLAB/Simulink is conducted to demonstrate the performance of the proposed HMMD control.

The remainder of this article is organized as follows. In Section II, the model of the four-wheel nonlinear coupled vehicle dynamics is developed, which includes the coupling relationship between the roll dynamics and the planar dynamics. In Section III, the decoupled nonlinear vehicle system is derived. In Section IV, the HMMD controller is developed, and the nominal dynamics are analyzed. Simulation results are presented and discussed in Section V, and conclusions of this article are drawn in Section VI.

II. Modeling of Nonlinear Vehicle Dynamics

The coupled vehicle body dynamics, including both vehicle planar and roll motions, are modeled in this section. Two common assumptions are made. First, small steering angles on the ground are assumed, so that $\sin\delta_k \approx 0$ and $\cos\delta_k \approx 1$, where δ is the steering angle, and the subscript $k \in \{f, r\}$ indicates the front wheel and rear wheel, respectively. Second, the vehicle is assumed to be bilaterally symmetric. Namely, the right and left sides of the steering angles and tire properties are the same.

A. Vehicle Body Dynamics Model

A 4-DOF vehicle dynamics model diagram is presented in Fig. 1, which includes vehicle longitudinal, lateral, yaw, and roll

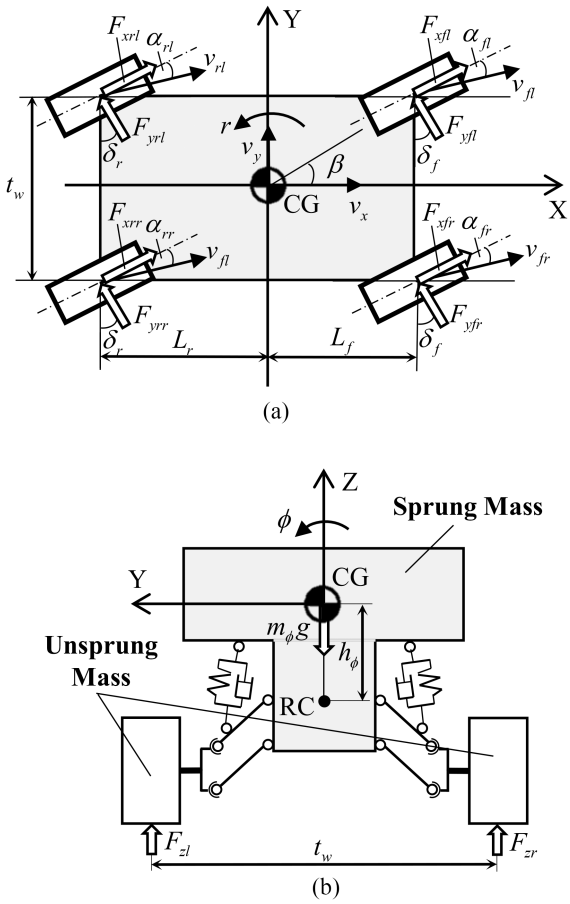

Fig. 1. Schematics of coupled nonlinear vehicle planar and roll dynamics.

motions. The four vehicle states corresponding to four DOFs are selected as:

1) v_x: longitudinal vehicle speed;
2) v_y: lateral vehicle speed;
3) r: yaw rate;
4) ϕ: roll angle.

In Fig. 1, β is the vehicle sideslip angle, m_ϕ is the vehicle sprung mass. L_f and L_r are the distances from the center of gravity (CG) to front and rear axles, respectively. t_w is the wheel track, h_ϕ is the distance from the CG to the roll center (RC). F_{xi} is the longitudinal tire force, where the subscript $i \in \{fl, fr, rl, rr\}$ indicates the front left, front right, rear left, and rear right wheels, respectively. F_{yi} is the lateral tire force of each wheel. F_{zl} and F_{zr} denote the left-side and right-side vertical tire forces, respectively. α_i is the slip angle of each wheel, and v_i is the forwarding speed of each wheel.

The coupled nonlinear vehicle dynamics model with the four vehicle states are described in (1) [18].

$$\begin{cases} \sum F_x = M\left(\dot{v}_x - r v_y\right) - m_\phi h_\phi \left(\phi \dot{r} + 2r\dot{\phi}\right) \\ \sum F_y = M\left(\dot{v}_y + r v_x\right) + m_\phi h_\phi \left(\ddot{\phi} - r^2 \phi\right) \\ \sum M_z = I_z \dot{r} - m_\phi h_\phi \left(\dot{v}_x - r v_y\right) \phi \\ \sum M_{x\phi} = \left(I_{x\phi} + m_\phi h_\phi^2\right) \ddot{\phi} + m_\phi h_\phi \left(\dot{v}_y + r v_x\right) \\ \quad - \left(m_\phi h_\phi^2 + I_{y\phi} - I_{z\phi}\right) r^2 \phi + \left(K_\phi - m_\phi h_\phi g\right) \phi \end{cases}, \quad (1)$$

where M denotes the vehicle total mass and K_ϕ denotes the roll stiffness. I_z is the overall vehicle yaw moment of inertia with respect to Z-axis. $I_{x\phi}$, $I_{y\phi}$, and $I_{z\phi}$ are the roll, pitch, and yaw moment of inertias about the sprung mass with respect to X-axis, Y-axis, and Z-axis, respectively. With the small steering angle assumption, $\sum F_x$, $\sum F_y$, $\sum M_z$, and $\sum M_{x\phi}$ are general forces and moments depicted in (2).

$$\begin{cases} \sum F_x = \sum_{i\in\{fl,fr,rl,rr\}} F_{xi} - F_{res} \\ \sum F_y = \sum_{i\in\{fl,fr,rl,rr\}} F_{yi} \\ \sum M_z = L_f\left(F_{yfl}+F_{yfr}\right) - L_r\left(F_{yrl}+F_{yrr}\right) - \Delta M_z \\ \sum M_{x\phi} = -C_\phi \dot{\phi} \end{cases} \tag{2}$$

where C_ϕ denotes the roll damping ratio, and F_{res} is the resistance force, which includes the air drag and the tire rolling resistance. ΔM_z is the additional corrective yaw moment generated by the difference of the longitudinal tire forces, which is presented in (3).

$$\Delta M_z = \frac{t_w}{2}\left[\left(F_{xfl}+F_{xrl}\right) - \left(F_{xfr}+F_{xrr}\right)\right]. \tag{3}$$

B. Tire Model

To accurately characterize the nonlinear tire forces, the magic formula tire model expressed in (4) is adopted [19].

$$\mathcal{Y} = s_d \sin\left\{s_c \arctan\left[s_b\mathcal{X} - s_e\left(s_b\mathcal{X} - \arctan s_b\mathcal{X}\right)\right]\right\}, \tag{4}$$

in which $\mathcal{Y}$ are longitudinal or lateral tire forces, F_x or F_y, respectively, with $\mathcal{X}$ accordingly being tire slip ratio or slip angle, respectively. s_b, s_c, s_d, and s_e are tire model parameters, which are calibrated by using CarSim tire data.

III. Decoupled Nonlinear Vehicle System

A. Feedback Linearization for Vehicle Roll Dynamics

A straightforward idea of converting the nonlinear vehicle roll dynamics in (1) to a controllable linear one is to cancel the nonlinear terms by designing a feedback control law. Substituting the second equation (e.g., the vehicle lateral dynamics) into the last equation in (1) to replace $\dot{v}_y$, the vehicle roll dynamics can be rewritten in (5).

$$k_2\ddot{\phi} + C_\phi\dot{\phi} + k_3\phi + \frac{k_1^2}{M}\left(r^2\phi - \ddot{\phi} + \frac{\sum F_y}{k_1}\right) - k_4 r^2\phi = 0, \tag{5}$$

where k_1, k_2, k_3 and k_4 are four constants defined in (6).

$$\begin{cases} k_1 = m_\phi h_\phi \\ k_2 = I_{x\phi} + m_\phi h_\phi^2 \\ k_3 = K_\phi - m_\phi h_\phi g \\ k_4 = m_\phi h_\phi^2 + I_{y\phi} - I_{z\phi} \end{cases}. \tag{6}$$

Selecting $x_1 = \phi, x_2 = \dot{\phi}$, and $u = \sum F_y/M$, the vehicle roll dynamics in (5) is reformulated in a state space model in (7).

$$\dot{\mathbf{x}} = A\mathbf{x} + B\left[u - \alpha(\mathbf{x})\right], \tag{7}$$

where $\mathbf{x} = [x_1, x_2]^{\mathrm{T}}$, and

$$A = \begin{bmatrix} 0 & 1 \\ -\frac{k_3}{k_2} & -\frac{C_\phi}{k_2} \end{bmatrix}, \tag{8}$$

$$B = \begin{bmatrix} 0 \\ k_1 \end{bmatrix}, \tag{9}$$

$$\alpha(\mathbf{x}) = \frac{1}{M}\left(k_1\dot{x}_2 + \frac{Mk_4 - k_1^2}{k_1} r^2 x_1\right). \tag{10}$$

Implied by the structure of (7), the vehicle roll dynamics in (5) is a linearizable feedback system. In this case, the following Theorem 1 provides the state feedback control law to linearize the vehicle roll dynamics. Namely, the input-output feedback linearization approach is applied to the single-input-single-output (SISO) vehicle roll dynamics.

Theorem 1 (Roll dynamics feedback linearization): Considering the nonlinear vehicle dynamics in (1), if the roll stiffness satisfies $K_\phi > m_\phi h_\phi g$, then the state feedback control law designed in (11) makes the linearized vehicle roll dynamics in (7) stable.

$$u = \alpha(\mathbf{x}). \tag{11}$$

Proof: Substituting the state feedback control law (7) to (11), the vehicle roll dynamics becomes

$$\dot{\mathbf{x}} = A\mathbf{x}. \tag{12}$$

The eigenvalues of A in (8) are

$$\upsilon_j = \frac{-C_\phi \pm \sqrt{C_\phi^2 - 4k_2k_3}}{2k_2}, j \in \{1,2\}. \tag{13}$$

Physically, the roll damping ratio C_ϕ and parameter k_2 are all positive. The condition in (14) also makes $k_3 > 0$,

$$K_\phi > m_\phi h_\phi g. \tag{14}$$

Hence, A is Hurwitz since the real parts of eigenvalues in (13) are all negative. The linearized roll dynamics in (12) is exponentially stable. ■

Remark 1: The inequality in (14) may need to be checked for different vehicle design case by case. However, the roll stiffness K_ϕ is typically a large value, i.e., 75545 N·m/rad [20], such that the condition $K_\phi > m_\phi h_\phi g$ in Theorem 1 is generally validated in practice, given that the value of h_ϕ is typically less than 1 for passenger cars.

B. MIMO Decoupling Matrix for Nonlinear Vehicle Dynamics

By utilizing the feedback control law (11) and the resulting linearized roll states (7), the nonlinear vehicle dynamics in (1) are reorganized as a square control-affine system in (15), which is a MIMO vehicle system.

$$\begin{cases} \dot{\tilde{\mathbf{x}}} = \mathbf{f}(\tilde{\mathbf{x}}) + \sum_{j=1}^{2} \mathbf{g}_j(\tilde{\mathbf{x}})\tilde{u}_j \\ \mathbf{y} = \mathbf{h}(\tilde{\mathbf{x}}) = [h_1, h_2]^{\mathrm{T}} \end{cases}, \tag{15}$$

in which $\tilde{\mathbf{x}} = [\tilde{x}_1, \tilde{x}_2, \tilde{x}_3, \tilde{x}_4, \tilde{x}_5]^{\mathrm{T}}$ denotes the vehicle states, and $\tilde{x}_1 = v_x, \tilde{x}_2 = v_y, \tilde{x}_3 = r, \tilde{x}_4 = \phi$, and $\tilde{x}_5 = \dot{\phi}$. $\tilde{u}_1 = \sum F_x/M$

and $\tilde{u}_2 = \sum M_z/I_z$ are the control inputs. $\mathbf{y} = [y_1, y_2]^{\mathrm{T}}$ denotes the output of the system, and $h_1 = \tilde{x}_2$, and $h_2 = \tilde{x}_3$. Moreover, $\mathbf{f}(\tilde{\mathbf{x}}) = [f_1, f_2, f_3, f_4, f_5]^{\mathrm{T}}$ and $\mathbf{g}_j(\tilde{\mathbf{x}})$ are defined in (16) and (17), respectively.

$$\begin{cases} f_1 = \frac{c_1\left(2\tilde{x}_5 - c_2\tilde{x}_2\tilde{x}_4^2\right) + \tilde{x}_2}{\kappa}\tilde{x}_3 \\ f_2 = \left(c_1 + c_3\right)\tilde{x}_3^2\tilde{x}_4 - \tilde{x}_1\tilde{x}_3 \\ f_3 = \frac{2c_1c_2\tilde{x}_3\tilde{x}_4\tilde{x}_5}{\kappa} \\ f_4 = \tilde{x}_5 \\ f_5 = c_4\tilde{x}_4 + c_5\tilde{x}_5 \end{cases}, \tag{16}$$

$$\begin{cases} \mathbf{g}_1(\tilde{\mathbf{x}}) = \left[\frac{1}{\kappa} \quad 0 \quad \frac{c_2\tilde{x}_4}{\kappa} \quad 0 \quad 0\right]^{\mathrm{T}} \\ \mathbf{g}_2(\tilde{\mathbf{x}}) = \left[\frac{c_1\tilde{x}_4}{\kappa} \quad 0 \quad \frac{1}{\kappa} \quad 0 \quad 0\right]^{\mathrm{T}} \end{cases}, \tag{17}$$

where κ is defined in (18).

$$\kappa = 1 - c_1c_2\tilde{x}_4^2. \tag{18}$$

Moreover, c_1, c_2, c_3, c_4, and c_5 are constants defined in (19).

$$\begin{cases} c_1 = \frac{k_1}{M} \\ c_2 = \frac{k_1}{I_z} \\ c_3 = \frac{Mk_4 - k_1^2}{k_1} \\ c_4 = -\frac{k_3}{k_2} \\ c_5 = -\frac{C_\phi}{k_2} \end{cases}. \tag{19}$$

Based on the vehicle physical properties, positive c_1 and c_2 are typically less than 1. Moreover, $\tilde{x}_4^2 \ll 1$ since the roll angle is usually a small angle with a unit in rad (in SI). Hence, $\kappa > 0$ and $1/\kappa$ is finite in (16) and (17).

Different from the feedback linearization process for vehicle roll states through (5)–(10), it is not straightforward to directly find the feedback control law for (15) by rewriting a form that is similar to (7). In other words, the input-output decoupling of the MIMO nonlinear vehicle dynamics in (15) demands a diffeomorphism such that the mapping relationship between the transformed inputs and outputs are linear and decoupled.

$$\begin{cases} \dot{y}_1 = \dot{\tilde{x}}_2 = \left(c_1 + c_3\right)\tilde{x}_3^2\tilde{x}_4 - \tilde{x}_1\tilde{x}_3 \\ y_1^{(2)} = \left(c_1 + c_3\right)\left(\frac{4c_1c_2\tilde{x}_3^2\tilde{x}_4^2\tilde{x}_5}{\kappa} + \tilde{x}_3^2\tilde{x}_5\right) \\ \quad -\tilde{x}_3^2\frac{c_1\left(2\tilde{x}_5 - c_2\tilde{x}_2\tilde{x}_4^2\right) + \tilde{x}_2}{\kappa} - \frac{2c_1c_2\tilde{x}_1\tilde{x}_3\tilde{x}_4\tilde{x}_5}{\kappa} \\ \quad + \left[\left(c_1 + c_3\right)2\tilde{x}_3\tilde{x}_4 - \tilde{x}_1\right]\frac{c_2\tilde{x}_4\tilde{u}_1 + \tilde{u}_2}{\kappa} \\ \quad -\tilde{x}_3\frac{\tilde{u}_1 + c_1\tilde{x}_4\tilde{u}_2}{\kappa} \end{cases}, \tag{20}$$

Indicated by the derivatives of y_1 in (20), the control inputs $\tilde{u}_1$ and $\tilde{u}_2$ appear in the second derivative of y_1. Hence, the smallest relative degree corresponding to y_1 is $\rho_1 = 2$. Similarly, the smallest relative degree corresponding to y_2 is $\rho_2 = 1$ since the first derivative of y_2 contains $\tilde{u}_1$ and $\tilde{u}_2$, which is shown in (21).

$$\dot{y}_2 = \dot{x}_3 = \frac{2c_1c_2\tilde{x}_3\tilde{x}_4\tilde{x}_5}{\kappa} + \frac{c_2\tilde{x}_4\tilde{u}_1 + \tilde{u}_2}{\kappa}. \tag{21}$$

Using the smallest relative degree ρ_1 and ρ_2, the decoupling matrix of the vehicle system (15) is constructed in (22), which represents the mapping relationship of the diffeomorphism.

$$D(\tilde{\mathbf{x}}) = \begin{bmatrix} L_{g_1}L_f^{\rho_1 - 1}h_1(\tilde{\mathbf{x}}) & L_{g_2}L_f^{\rho_1 - 1}h_1(\tilde{\mathbf{x}}) \\ L_{g_1}L_f^{\rho_2 - 1}h_2(\tilde{\mathbf{x}}) & L_{g_2}L_f^{\rho_2 - 1}h_2(\tilde{\mathbf{x}}) \end{bmatrix}_{2\times 2}, \tag{22}$$

where L represents the *Lie Derivative* as stated in [21], and each element of $D(\tilde{\mathbf{x}})$ in (22) is described as,

$$\begin{cases} L_{g_1}L_f^{\rho_1 - 1}h_1(\tilde{\mathbf{x}}) = \frac{1}{\kappa}\left\{c_2\tilde{x}_4\left[2\left(c_1 + c_3\right)\tilde{x}_3\tilde{x}_4 - \tilde{x}_1\right] - \tilde{x}_3\right\} \\ L_{g_2}L_f^{\rho_1 - 1}h_1(\tilde{\mathbf{x}}) = \frac{1}{\kappa}\left[\left(c_1 + 2c_3\right)\tilde{x}_3\tilde{x}_4 - \tilde{x}_1\right] \\ L_{g_1}L_f^{\rho_2 - 1}h_2(\tilde{\mathbf{x}}) = \frac{1}{\kappa}c_2\tilde{x}_4 \\ L_{g_2}L_f^{\rho_2 - 1}h_2(\tilde{\mathbf{x}}) = \frac{1}{\kappa} \end{cases}. \tag{23}$$

Hence, the decoupling matrix $D(\tilde{\mathbf{x}})$ in (22) varies with respect to $\tilde{x}_1$, $\tilde{x}_3$, and $\tilde{x}_4$.

The existence of the decoupling control solution of the MIMO nonlinear system is equivalent to the non-singularity of the decoupling matrix $D(\tilde{\mathbf{x}})$ [21]. Namely, the diffeomorphism requires $D(\tilde{\mathbf{x}})$ being invertible. The following Theorem 2 claims a necessary and sufficient condition that the nonlinear vehicle dynamics (15) can be decoupled by $D(\tilde{\mathbf{x}})$.

Theorem 2 (MIMO Vehicle Dynamics Decoupling): Given that $1/\kappa$ is finite, the vehicle system in (15) can be decoupled by the decoupling matrix $D(\tilde{\mathbf{x}})$ if and only if $\tilde{x}_3(t) \neq 0$ for all $t > 0$.

Proof: First, (15) can be decoupled if and only if $D(\tilde{\mathbf{x}})$ is non-singular for all $t > 0$, which is equivalent to $\mathrm{rank}(D(\tilde{\mathbf{x}})) \equiv 2$.

Since $\kappa \neq 0$, the reduced form of $D(\tilde{\mathbf{x}})$ by removing the same factor $1/\kappa$ is described in (24).

$$D(\tilde{\mathbf{x}}) = \begin{bmatrix} c_2\tilde{x}_4\Theta - \tilde{x}_3 & \Theta - c_1\tilde{x}_3\tilde{x}_4 \\ c_2\tilde{x}_4 & 1 \end{bmatrix}_{2\times 2}, \tag{24}$$

where $\Theta = 2(c_1 + c_3)\tilde{x}_3\tilde{x}_4 - \tilde{x}_1$. On one hand, when $\tilde{x}_4 = 0$, $D(\tilde{\mathbf{x}})$ can be reduced as the upper triangular matrix in (25).

$$D(\tilde{\mathbf{x}}) = \begin{bmatrix} -\tilde{x}_3 & -\tilde{x}_1 \\ 0 & 1 \end{bmatrix}_{2\times 2}. \tag{25}$$

In this case, $\mathrm{rank}(D(\tilde{\mathbf{x}})) \equiv 2$ is held if and only if $\tilde{x}_3 \neq 0$. On the other hand, when $\tilde{x}_4 \neq 0$, $\mathrm{rank}(D(\tilde{\mathbf{x}})) \equiv 2$ is held if and only if two row vectors of $D(\tilde{\mathbf{x}})$ in (24) are linear independent. Namely, when $\tilde{x}_3 \neq 0$, the two row vectors are independent. ■

Remark 2: Implied by Theorem 2, requiring $\tilde{x}_3(t) \neq 0$ suggests that the proposed decoupling control will not work with zero yaw rate. Generally, the decoupling control can only be activated when lateral vehicle dynamics are displayed through steering commands (e.g., a cornering or lane changing maneuver). Therefore, a control trigger based on the vehicle states feedback is required to prevent $D(\tilde{\mathbf{x}})$ from being singular.

C. Vehicle Input-Output Model

Together with the smallest relative degrees, ρ_1 and ρ_2, and the nonsingular decoupling matrix $D(\tilde{\mathbf{x}})$, the decoupled vehicle

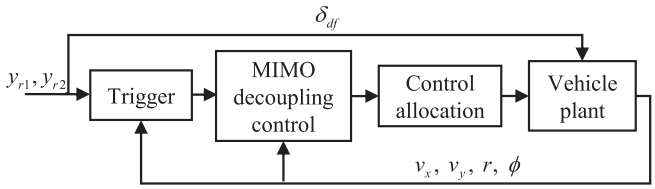

Fig. 2. Control configuration of the HMMD control.

input-output model of (15) can be established as (26).

$$\mathbf{y}^{\rho_1,\rho_2} = \begin{bmatrix} \frac{\mathrm{d}^{\rho_1} y_1}{\mathrm{d}t^{\rho_1}} \\ \frac{\mathrm{d}^{\rho_2} y_2}{\mathrm{d}t^{\rho_2}} \end{bmatrix} = C(\tilde{\mathbf{x}}) + D(\tilde{\mathbf{x}})\tilde{\mathbf{u}}, \tag{26}$$

where $\tilde{\mathbf{u}} = [\tilde{u}_1, \tilde{u}_2]^{\mathrm{T}}$, and $C(\tilde{\mathbf{x}})$ is depicted in (27).

$$C(\tilde{\mathbf{x}}) = \begin{bmatrix} L_f^{\rho_1} h_1(\tilde{\mathbf{x}}) \\ L_f^{\rho_2} h_2(\tilde{\mathbf{x}}) \end{bmatrix}, \tag{27}$$

in which

$$\begin{cases} L_f^{\rho_1} h_1(\tilde{\mathbf{x}}) = -\tilde{x}_3^2 \frac{c_1\left(2\tilde{x}_5 - c_2\tilde{x}_2\tilde{x}_4^2\right) + \tilde{x}_2}{\kappa} \\ \qquad\qquad + \left[2\left(c_1 + c_3\right)\tilde{x}_3\tilde{x}_4 - \tilde{x}_1\right] \frac{2c_1c_2\tilde{x}_3\tilde{x}_4\tilde{x}_5}{\kappa} \\ \qquad\qquad + \left(c_1 + c_3\right)\tilde{x}_3^2\tilde{x}_5 \\ L_f^{\rho_2} h_2(\tilde{\mathbf{x}}) = \frac{2c_1c_2\tilde{x}_3\tilde{x}_4\tilde{x}_5}{\kappa} \end{cases}. \tag{28}$$

IV. Hierarchical Controller Design

The overview of the proposed HMMD controller is presented in Fig. 2, in which δ_{df} is the feedforward front steering angle input, and y_{r1} and y_{r2} are the references of y_1 and y_2, respectively. The HMMD control intends to track the references of vehicle lateral speed and yaw rate, and simultaneously mitigate rollover propensity by reducing the values of rollover indexes, such as load transfer ratio (LTR) [8], [9]. For an over-actuated vehicle with multiple electric driving/braking motors and front and rear steering motors [4], a control allocation module is typically applied to distribute the virtual control efforts obtained from the high-level MIMO decoupling design. Moreover, according to Remark 2, a state feedback-based trigger is designed for the feedback control to avoid the singularity of the decoupling matrix and unexpected chattering effects of control.

A. High-Level Virtual Controller Design

Given the condition $\tilde{x}_3(t) \neq 0$ in Theorem 2, the feedback control law can be directly obtained via (26) to achieve the input-output decoupling, which is shown in (29).

$$\tilde{\mathbf{u}} = D^{-1}(\tilde{\mathbf{x}})\left(\mathbf{v} - C(\tilde{\mathbf{x}})\right), \tag{29}$$

where $\mathbf{v} = [v_1, v_2]^{\mathrm{T}}$ is the synthetic control input. Substituting (26) into (29), we have (30),

$$\mathbf{y}^{\rho_1,\rho_2} = \mathbf{v}. \tag{30}$$

The references y_{r1} and y_{r2} are defined as the first order delay system by the transfer function in (31), [22].

$$\begin{cases} y_{r1} = 0 \\ y_{r2} = \frac{\kappa_r}{1+\tau_r s}\delta_f \end{cases}, \tag{31}$$

in which

$$\kappa_r = \frac{v_x}{L_f + ML_f v_x^2 / 2C_{yf}L_f\left(L_f + L_r\right)}, \tag{32}$$

$$\tau_r = \frac{v_x I_z}{ML_r v_x^2 + 2C_{yf}L_f\left(L_f + L_r\right)}, \tag{33}$$

where $C_{yf} = C_{yfl} = C_{yfr}$ is the equivalent tire cornering stiffness of the front axle based on the bilateral symmetry assumption. In addition, the equivalent tire corning stiffness can be estimated from the linear range of the nonlinear tire model (4) for the reference model.

To track the references y_{r1}, y_{r2}, and stabilize the dynamics in (30), the synthetic control inputs are designed in (34), which includes a stabilization part and a tracking part. The stabilization part has been proved to make (30) Hurwitz stable in [23], and the tracking part is a proportional–integral controller to dismiss reference tracking errors.

$$\begin{cases} v_1 = \underbrace{-\alpha_1^1 h_1(\tilde{\mathbf{x}}) - \alpha_2^1 L_f h_1(\tilde{\mathbf{x}})}_{\text{Stabilization}} + \underbrace{K_P^1 e_1 + K_I^1 \int e_1}_{\text{Tracking}} \\ v_2 = \underbrace{-\alpha_1^2 h_2(\tilde{\mathbf{x}})}_{\text{Stabilization}} + \underbrace{K_P^2 e_2 + K_I^2 \int e_2}_{\text{Tracking}} \end{cases}, \tag{34}$$

where α_1^1, α_2^1, α_1^2, K_P^1, K_I^1, K_P^2, and K_I^2 are positive control gains. e_1 and e_2 are two tracking errors defined in (35).

$$e_m = y_{rm} - y_m, m \in \{1, 2\}. \tag{35}$$

B. Nominal Stability Analysis

The diffeomorphism of $\tilde{\mathbf{x}}$ is depicted in (36).

$$\mathbf{z} = \Phi(\tilde{\mathbf{x}}) = \begin{bmatrix} \xi \\ \eta \end{bmatrix}. \tag{36}$$

Given the sum of the individual smallest relative degree $\rho = \rho_1 + \rho_2$, ξ is the first ρ coordinates in $\Phi(\tilde{\mathbf{x}})$, which is presented in (37).

$$\begin{aligned} \xi &= \begin{bmatrix} \xi_1^1(\tilde{\mathbf{x}}) & \xi_2^1(\tilde{\mathbf{x}}) & \xi_1^2(\tilde{\mathbf{x}}) \end{bmatrix}^{\mathrm{T}} \\ &= \begin{bmatrix} h_1(\tilde{\mathbf{x}}) & L_f h_1(\tilde{\mathbf{x}}) & h_2(\tilde{\mathbf{x}}) \end{bmatrix}^{\mathrm{T}}. \end{aligned} \tag{37}$$

Besides, η is the rest of the $n - \rho$ coordinates in $\Phi(\tilde{\mathbf{x}})$, where n is the number of the DOFs of $\tilde{\mathbf{x}}$. η is depicted in (38).

$$\begin{aligned} \eta &= \begin{bmatrix} \eta_1(\tilde{\mathbf{x}}) & \eta_2(\tilde{\mathbf{x}}) \end{bmatrix}^{\mathrm{T}} \\ &= \begin{bmatrix} \tilde{x}_4 & \tilde{x}_5 \end{bmatrix}^{\mathrm{T}}. \end{aligned} \tag{38}$$

Applying the diffeomorphism $\Phi(\tilde{\mathbf{x}})$, the vehicle system in (15) is rewritten into the form in (39), which is a decoupled

linear system.

$$\begin{cases} \dot{\xi} = H\xi + K\mathbf{v} \\ \dot{\eta} = Q(\eta,\xi) + P(\eta,\xi)\tilde{\mathbf{u}} \end{cases}, \tag{39}$$

where H, K, $Q(\eta,\xi)$, and $P(\eta,\xi)$ are defined in (40).

$$\begin{cases} H = \begin{bmatrix} 0 & 1 & 0 \\ 0 & 0 & 0 \\ 0 & 0 & 0 \end{bmatrix} \\ K = \begin{bmatrix} 0 & 0 \\ 1 & 0 \\ 0 & 1 \end{bmatrix} \\ Q(\eta,\xi) = \begin{bmatrix} L_f\eta_1(\tilde{\mathbf{x}}) \\ L_f\eta_2(\tilde{\mathbf{x}}) \end{bmatrix}\Big|_{\tilde{\mathbf{x}}=\Phi^{-1}(\mathbf{z})} = \begin{bmatrix} \eta_2 \\ c_4\eta_1 + c_5\eta_2 \end{bmatrix} \\ P(\eta,\xi) = \begin{bmatrix} L_{g_1}\eta_1(\tilde{\mathbf{x}}) & L_{g_2}\eta_1(\tilde{\mathbf{x}}) \\ L_{g_1}\eta_2(\tilde{\mathbf{x}}) & L_{g_2}\eta_2(\tilde{\mathbf{x}}) \end{bmatrix}\Big|_{\tilde{\mathbf{x}}=\Phi^{-1}(\mathbf{z})} = \mathbf{0}_{2\times 2} \end{cases}, \tag{40}$$

in which $\tilde{\mathbf{x}} = \Phi^{-1}(\mathbf{z}) = \left[(c_1+c_2)\xi_1^2\eta_1 - \frac{\xi_2^1}{\xi_1^2}, \xi_1^1, \xi_1^2, \eta_1, \eta_2\right]^{\mathrm{T}}$.

The nominal stability of the decoupled system (39) is indicated by its output zero dynamics, which is associated with internal zero dynamics. The decoupled system is stable, namely the minimum phase, as long as the output zero dynamics is stable [21], [23].

Defining the internal zero dynamics as $\xi = \mathbf{0}_{3\times 1}$, we have $\mathbf{y}^{\rho_1,\rho_2} = \mathbf{0}_{2\times 1}$, and the control law in (29) becomes $\tilde{\mathbf{u}} = -D^{-1}(\tilde{\mathbf{x}})C(\tilde{\mathbf{x}})$. Therefore, the output zero dynamics are given by (41), considering $P = \mathbf{0}_{2\times 2}$ in (40),

$$\begin{aligned} \dot{\eta} &= Q(\eta,0) - P(\eta,0)D^{-1}(\eta,0)C(\eta,0) \\ &= Q(\eta,0) \\ &= \begin{bmatrix} \eta_2 \\ c_4\eta_1 + c_5\eta_2 \end{bmatrix}. \end{aligned} \tag{41}$$

From (8) and (19), the output dynamics in (41) is exactly the same as the decoupled roll dynamics in (12), which is proved in Theorem 1 that the equilibrium point is exponentially stable. Therefore, the system in (41) is stable and is in the minimum phase since the zero dynamics have an asymptotical equilibrium point in the domain of interest.

C. Control Allocation

Integrating the feedback linearization of the vehicle roll dynamics and the MIMO decoupling control of the vehicle planar dynamics, the high-level virtual control input of the HMMD controller is $\tau_c = [u, \tilde{u}_1, \tilde{u}_2]^{\mathrm{T}}$, which is determined by the control laws in (11) and (29). Employing the low-level actuators, the over-actuated vehicle with four-wheel steering and four-IWMs demands the real control inputs, including the front and rear steering angles and the driving torque/force of each IWM. Namely, the low-level real control input is $\hat{u} = [\delta_f, \delta_r, F_{xfl}, F_{xfr}, F_{xrl}, F_{xrr}]^{\mathrm{T}}$, in which $\delta_f = \delta_{df} + \Delta\delta_f$, and $\Delta\delta_f$ is the additional front-wheel steering angle by considering the feedforward front steering angle δ_{df}. Moreover, the additional rear-wheel steering angle $\Delta\delta_r$ equals to δ_r since there is no feedforward rear-wheel steering given by human drivers. Therefore, the control allocation is applied to distribute the high-level virtual control τ_c to the low-level real control input $\hat{u}$ since the dimension of $\hat{u}$ is larger than that of τ_c. Incorporating all the actuators together, the mapping relationship between $\hat{u}$ and the achievable values of τ_c, denoted as τ, are formulated in (42) by substituting (2), (3), and (4).

$$\tau = \begin{bmatrix} \sum F_y/M \\ \sum F_x/M \\ \sum M_z/I_z \end{bmatrix} = S\hat{u}, \tag{42}$$

where S is the mapping matrix as shown in (43).

$$S = \begin{bmatrix} \frac{2C_{yf}}{M} & \frac{2C_{yr}}{M} & 0 & 0 & 0 & 0 \\ 0 & 0 & \frac{1}{M} & \frac{1}{M} & \frac{1}{M} & \frac{1}{M} \\ \frac{2L_fC_{yf}}{I_z} & -\frac{2L_rC_{yr}}{I_z} & \frac{t_w}{2I_z} & \frac{t_w}{2I_z} & -\frac{t_w}{2I_z} & -\frac{t_w}{2I_z} \end{bmatrix} \tag{43}$$

where $C_{yr} = C_{yrl} = C_{yrr}$ is the equivalent tire cornering stiffness of the rear axle.

The control allocation problem is formulated in (44).

$$\begin{aligned} &\min_{\hat{u}} J = \|\hat{u}\|_{W_1} + \|\tau(\hat{u}) - \tau_c\|_{W_2} \\ &\text{s.t.} \begin{cases} \hat{u} \in U \\ \tau(\hat{u}) = S\hat{u} \end{cases} \end{aligned} \tag{44}$$

where W_1 and W_2 are two weighting matrices, which are applied to normalize the two terms with different units in the cost function for the numerical optimization. U is the feasible region of $\hat{u}$, which depends on the physical capability of the actuators. For steering angles, $\delta_f, \delta_r \in [-30^\circ, 30^\circ]$. For tire longitudinal forces, $F_{xfl}, F_{xfr}, F_{xrl}, F_{xrr} \in [-3000\mathrm{N}, 3000\mathrm{N}]$.

D. Control Trigger

A control trigger is necessary to guarantee the feasibility of the MIMO decoupling control based on Theorem 2. The MIMO decoupling control will only work when the controlled vehicle showing lateral dynamics with non-zero yaw rate.

Furthermore, a rollover index, the lateral load transfer ratio (LTR), is also involved in the prevention of vehicle rollover [24]. Generally, larger LTR values represent a higher rollover propensity of vehicles, so that a constant threshold of the LTR is employed in the trigger [24]. Under this condition, the decoupling controller with a constant LTR threshold may be frequently turned on and off due to various driving maneuvers. Consequently, the frequent switches will not only provide discontinuous control efforts but also cause/excite unexpected chattering of vehicle states. To avoid this situation, a dynamic weighting method in the trigger is applied to smooth the control efforts. The design of the trigger is depicted in (45), in which the value of $\mathcal{T}$ varies from 0 to 1.

$$\mathcal{T} = \mathrm{sgn}\left(|r|\right) \cdot w\left(|LTR|\right), \tag{45}$$

where $\mathrm{sgn}(|r|)$ is the sign function, and the estimation of $LTR \in [-1, 1]$ is shown in (46), [25]. In addition, $w(\cdot)$ denotes the dynamic weighting function shown in (47), where $\varepsilon \in (0, 1)$

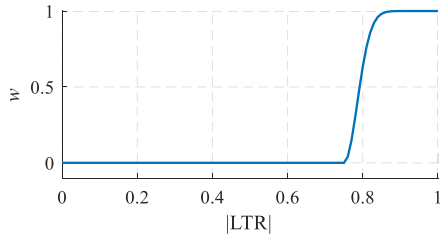

Fig. 3. Dynamic weighting function.

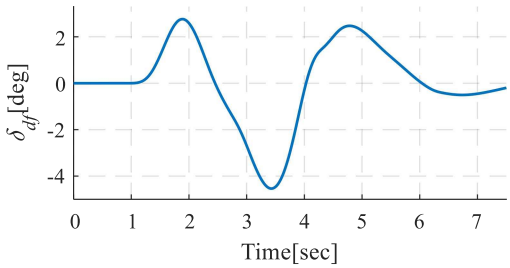

Fig. 4. Driver steering angle input of the DLC maneuver.

and σ are two constants that can be calibrated.

$$LTR = \frac{2m_\phi h_\phi}{Mt_w}\left[\frac{(\dot{v}_y + rv_x)\cos\phi}{g} + \sin\phi\right]. \tag{46}$$

$$w\left(|LTR|\right) = \begin{cases} 0 & |LTR| \le \varepsilon \\ 1 - \exp\left[-\left(\frac{|LTR|-\varepsilon}{\sigma}\right)^2\right] & |LTR| > \varepsilon \end{cases}, \tag{47}$$

In detail, ε indicates the lower LTR bound for non-zero value of w, and σ helps to determine the slop of the rising curve of non-zero value of w. Fig. 3 illustrates the trend of $w(|LTR|)$ with $\sigma = 0.05$, which starts from 0 and activates the controller at $\varepsilon = 0.75$.

From (45), $\mathcal{T} = 0$ implies the controller is turned off when either $\mathrm{sgn}(|r|)$ or $w(|LTR|)$ is zero. On one hand, $\mathrm{sgn}(|r|)$ can disable the controller with $r = 0$ for a straight-line driving, which ensure that the condition in Theorem 2 holds. On the other hand, $w(|LTR|)$ provides a continuous control weight to smooth control inputs activated by LTR.

Applying the trigger, the final virtual control input can be rewritten as (48).

$$\tau_c = \mathcal{T} \cdot [u, \tilde{u}_1, \tilde{u}_2]^{\mathrm{T}}. \tag{48}$$

V. Simulation Results and Discussions

In this section, the co-simulations are conducted via integrated CarSim and MATLAB/Simulink to demonstrate the performance of the proposed HMMD controller. In CarSim, an E-class SUV with high-fidelity vehicle parameters is selected as the simulated vehicle. Moreover, a double-lane change (DLC) maneuver is commanded on the road with a tire-road friction coefficient at 0.85. Fig. 4 shows the driver steering angle input δ_{df} of the DLC maneuver. The targeted driving speed is 120 km/h. The proposed HMMD controller is implemented in MATLAB/Simulink. In addition, the optimization problem of the control allocation is solved by the constrained optimization command (fmincon) with the active set algorithm. The vehicle parameters are listed in Table I.

TABLE I
Values of Vehicle Parameters and Simulations

Parameters	Values	Parameters	Values
M	1710 kg	α	1
m_ϕ	1590 kg	K_P^1	0.1
I_z	2889.9 kg/m^2	K_I^1	0.2
$I_{x\phi}$	894.4 kg/m^2	K_P^2	2
$I_{y\phi}$	2687.1 kg/m^2	K_I^2	0.5
$I_{z\phi}$	2687.1 kg/m^2	W_1	diag(10000,10000,1,1,1,1)*
L_f	1.18 m	W_2	diag(1,20,1)
L_r	1.77 m	C_{yf}	60000 N/rad
t_w	1.575 m	C_{yr}	60000 N/rad
h_ϕ	0.3 m		

*diag: diagonal matrix

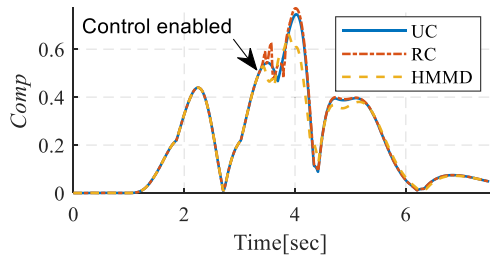

Fig. 5. Simulation responses of the comprehensive index.

For comparisons, an uncontrolled vehicle is used as a benchmark. In addition, the vehicle only with the rollover prevention control law (11) is also simulated to verify that it is necessary to have additional MIMO decoupling control to mitigate oscillatory coupling responses and maintain vehicle planar motion stability. The uncontrolled vehicle and the vehicle only with the rollover control are also with the same initial conditions and parameters of the vehicle steered by the HMMD controller. The dynamic weighting function presented in (45) with $\sigma = 0.05$ and $\varepsilon = 0.75$ is applied to both vehicles with only rollover control and the HMMD controller.

To demonstrate the comprehensive performance of the MIMO decoupling control, a new nondimensionalized comprehensive index, $Comp$, is developed in (49), in which the LTR defined in (46) represents roll stability, and e_m defined in (35) indicates yaw and lateral stability. From (49), a small value of $Comp$ is anticipated for a desired control performance.

$$Comp = \frac{1}{3}\left(\frac{|LTR|}{\max\left(|LTR|\right)} + \sum_{m=1}^{2}\frac{|e_m|}{\max\left(|e_m|\right)}\right) \tag{49}$$

The simulation results of three cases are shown in Figs. 5 –12. The legends "UC" and "RC" represent the uncontrolled vehicle and the vehicle with only rollover control law (11), respectively. The results of $Comp$ responses are displayed in Table II and

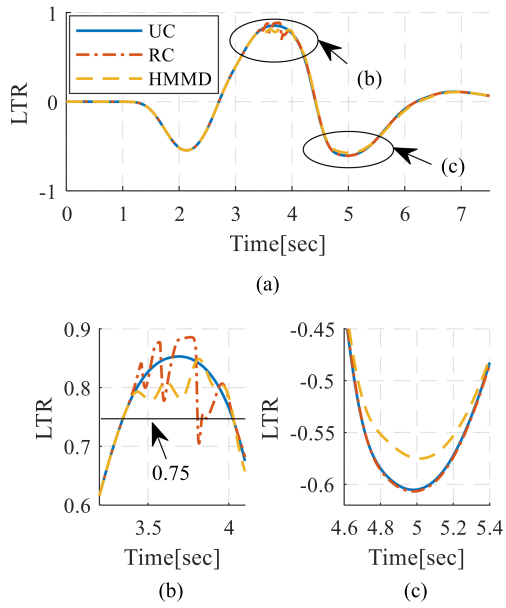

Fig. 6. Simulation responses of the LTR.

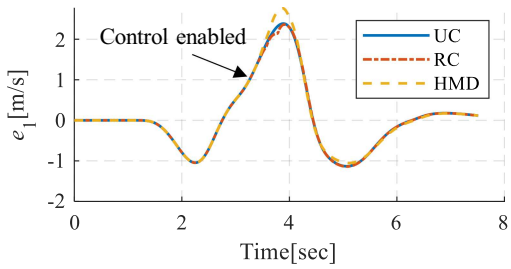

Fig. 7. Simulation responses of the lateral speed tracking error.

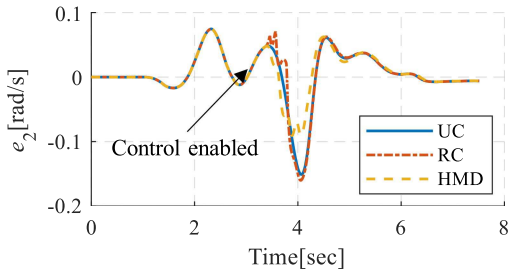

Fig. 8. Simulation responses of the yaw rate tracking error.

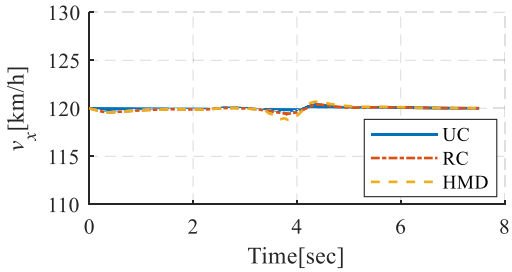

Fig. 9. Simulation responses of the longitudinal speed.

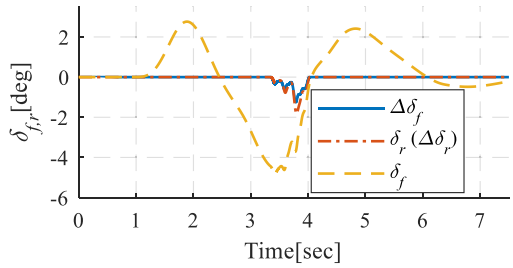

Fig. 10. Steering angles inputs after the control allocation.

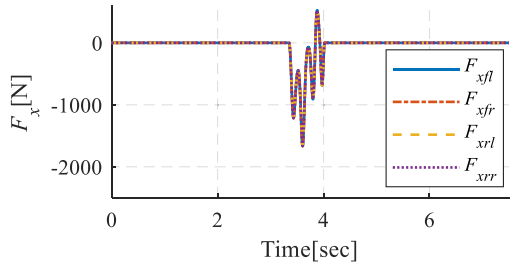

Fig. 11. Longitudinal tire forces after the control allocation.

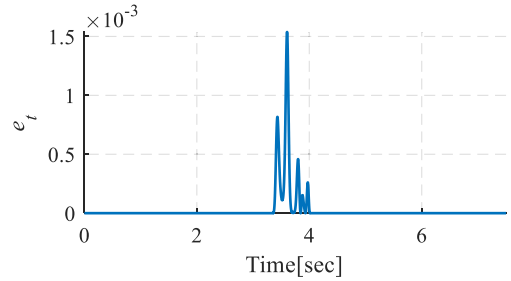

Fig. 12. Tracking errors of the virtual controls in the control allocation.

TABLE II
STATISTICAL EVALUATION OF THE COMPREHENSIVE INDEX

Case	Time Integration*	Mean*	Variance*
UC	1.5627	0.2684	0.0380
RC	1.5821	0.2717	0.0399
HMMD	**1.5030**	**0.2586**	**0.0317**

*: The values are calculated after the HMMD controller enabled.

Fig. 5. The HMMD controller is activated during 3.2 s–4.1 s. The "HMMD" vehicle has smaller values of the comprehensive index, compared with the results of the "UC" and "RC" vehicle. In addition, based on the statistical evaluations in Table II, the "HMMD" vehicle also can achieve smallest time integration, mean, and variance. Therefore, the proposed HMMD can process better control performance by considering vehicle roll stability and lateral/yaw stability simultaneously.

The LTR responses of the three cases are shown in Fig. 6. Owing to the steering maneuver, Fig. 6(a) indicates that high rollover propensities appear during 3.2 s–4.1 s and 4.6 s–5.4 s, which are presented in the zoom-in plots of Fig. 6(b) and (c), respectively. From Fig. 6(b) and (c), the "UC" vehicle is stable without rollover happening, but it has high rollover propensity since the values of the LTR approach to 0.9 and –0.6. However,

compared with the "UC" vehicle, the HMMD controller can mitigate vehicle rollover propensity when the value of the LTR exceeds the trigger threshold 0.75. In addition, while the "RC" vehicle also tries to depress the LTR, the chattering behavior emerges in Fig. 6(b), which results in the worse/larger LTR responses than the ones in the "UC" case. That is because the oscillatory coupling dynamics is not considered in the "RC" vehicle. Therefore, the HMMD controller can enhance vehicle anti-rollover performance as well as deal with oscillatory coupling behaviors.

The lateral and yaw state tracking performances of vehicles are presented in Figs. 7 and 8, which imply the stability of vehicle planar motion. In Fig. 7, the tracking errors of vehicle lateral speed are presented. Although the "HMMD" vehicle has a little larger error after the controller enabled, it does not mean a worse lateral stability when the 4WS control is introduced. With an additional rear-steering angle, the vehicle lateral stability region is enlarged as the front and rear steering angles with the same direction are applied [26], [27], which is further verified in the plots of steering angles later. In Fig. 8, compared with the "UC" vehicle, the "RC" vehicle has larger tracking errors of yaw rate so that the "RC" vehicle sacrifices the yaw stability to fulfill the rollover prevention. However, the "HMMD" vehicle can achieve better yaw rate tracking performance than the "UC" and "RC" vehicles since the additional MIMO decoupling control involves the maintenance of yaw stability. The responses of vehicle longitudinal speed are displayed in Fig. 9, in which the targeted longitudinal speed 120 km/h is closely maintained.

The control allocation is only conducted in the HMMD controller, and Figs. 10 and 11 present the real control inputs after control allocation. From Figs. 10 and 11, all additional steering angles and longitudinal tire forces are within reasonable regions. Hence, the control inputs are practical for future engineering applications. In particular, $\Delta\delta_f$ and $\Delta\delta_r$ displayed in Fig. 10 make δ_f and δ_r steer in the same direction. Hence, the lateral stability region of the "HMMD" vehicle is enlarged, so that the corresponding larger e_1 during 3.2 s – 4.1 s in Fig. 7 is acceptable.

The tracking errors of the virtual controls in the control allocation e_t are shown in Fig. 12, which is the second penalty term in the cost function of (44). From Fig. 12, the maximum e_t is less than 1.6×10^{-3}. Hence, the control allocation can satisfy the virtual control inputs with high accuracy. To further validate the proposed control method, which is not limited to simulation, an experimental validation will be conducted through a collaboration with an auto company.

VI. Conclusion

This article studies the HMMD controller with the control trigger to address the oscillatory coupling behaviors of the planar and roll dynamics. The derived control laws can decouple vehicle roll and planar dynamics. In addition, the nominal stability of the decoupled system is also proved via the stability of the output zero dynamics.

Demonstrated by the co-simulation integrating CarSim and MATLAB/Simulink, the HMMD controller can achieve the smallest statistical evaluation values of the comprehensive index and suppress the vehicle rollover propensity by simultaneously ensuring vehicle planar stability without oscillations. The chatting issue of control efforts is also resolved. Moreover, the control allocation in the hierarchical configuration can generate reasonable real control inputs and track the virtual control inputs with high accuracy. The future work of the proposed research would investigate the real-time feasibility of the HMMD controller. Field experiments with a real vehicle will also be conducted for demonstration.

References

[1] S. Murata, "Innovation by in-wheel-motor drive unit," *Veh. Syst. Dyn.*, vol. 50, no. 6, pp. 807–830, 2012.

[2] H. Wang, H. Kong, Z. Man, D. M. Tuan, Z. Cao, and W. Shen, "Sliding mode control for steer-by-wire systems with AC motors in road vehicles," *IEEE Trans. Ind. Electron.*, vol. 61, no. 3, pp. 1596–1611, Mar. 2014.

[3] A. M. Dizqah, B. Lenzo, A. Sorniotti, P. Gruber, S. Fallah, and J. D. Smet, "A fast and parametric torque distribution strategy for four-wheel-drive energy-efficient electric vehicles," *IEEE Trans. Ind. Electron.*, vol. 63, no. 7, pp. 4367–4376, Jul. 2016.

[4] Y. Huang, F. Wang, A. Li, Y. Shi, and Y. Chen, "Development and performance enhancementof an overactuated autonomous ground vehicle," *IEEE/ASME Trans. Mechatronics*, vol. 26, no. 1, pp. 33–44, Feb. 2021, doi: 10.1109/TMECH.2020.2998454.

[5] R. Wang, Y. Chen, D. Feng, X. Huang, and J. Wang, "Development and performance characterization of an electric ground vehicle with independently actuated in-wheel motors," *J. Power Sources*, vol. 196, no. 8, pp. 3962–3971, 2011.

[6] Y. Chen and J. Wang, "Adaptive energy-efficient control allocation for planar motion control of over-actuated electric ground vehicles," *IEEE Trans. Control Syst. Technol.*, vol. 22, no. 4, pp. 1362–1373, Jul. 2014.

[7] F. Wang and Y. Chen, "Dynamics and control of a novel active yaw stabilizer to enhance vehicle lateral motion stability," *J. Dyn. Syst., Meas., Control*, vol. 140, no. 8, 2018, Art. no. 081007.

[8] F. Wang and Y. Chen, "A novel active rollover prevention for ground vehicles based on continuous roll motion detection," *J. Dyn. Syst., Meas. Control*, vol. 141, no. 1, 2019, Art. no. 011010.

[9] R. Rajamani, "Roll dynamics and rollover prevention," in *Vehicle Dynamics and Control*, 2nd ed. Berlin, Germany: Springer, 2012, pp. 427–456.

[10] J. Yoon, D. Kim, and K. Yi, "Design of a rollover index-based vehicle stability control scheme," *Veh. Syst. Dyn.*, vol. 45, no. 5, pp. 459–475, 2007.

[11] M. B. Alberding, J. Tjønnås, and T. A. Johansen, "Integration of vehicle yaw stabilization and rollover prevention through nonlinear hierarchical control allocation," *Veh. Syst. Dyn.*, vol. 52, no. 12, pp. 1607–1621, 2014.

[12] L. Li, Y. Lu, R. Wang, and J. Chen, "A three-dimensional dynamics control framework of vehicle lateral stability and rollover prevention via active braking with MPC," *IEEE Trans. Ind. Electron.*, vol. 64, no. 4, pp. 3389–3401, Apr. 2017.

[13] M. Ataei, A. Khajepour, and S. Jeon, "Model predictive control for integrated lateral stability, traction/braking control, and rollover prevention of electric vehicles," *Veh. Syst. Dyn.*, vol. 58, no. 1, pp. 49–73, 2020.

[14] R. Marino and F. Cinili, "Input–output decoupling control by measurement feedback in four-wheel-steering vehicles," *IEEE Trans. Control Syst. Technol.*, vol. 17, no. 5, pp. 1163–1172, Sep. 2009.

[15] H. Zhang and W. Zhao, "Decoupling control of steering and driving system for in-wheel-motor-drive electric vehicle," *Mech. Syst. Signal Process.*, vol. 101, pp. 389–404, 2018.

[16] R. Marino and S. Scalzi, "Asymptotic sideslip angle and yaw rate decoupling control in four-wheel steering vehicles," *Veh. Syst. Dyn.*, vol. 48, no. 9, pp. 999–1019, 2010.

[17] M. Li, Y. Jia, and J. Du, "LPV control with decoupling performance of 4WS vehicles under velocity-varying motion," *IEEE Trans. Control Syst. Technol.*, vol. 22, no. 5, pp. 1708–1724, Sep. 2014.

[18] F. Wang and Y. Chen, "Hierarchical input-output decoupling control for vehicle rollover mitigation," in *Proc. ASME Dyn. Syst. Control Conf.*, 2018, Paper DSCC20189166.

[19] H. B. Pacejka, *Tire and Vehicle Dynamics*. Amsterdam, The Netherlands: Elsevier, 2004.

[20] J. Ryu, E. J. Rossetter, and J. C. Gerdes, "Vehicle sideslip and roll parameter estimation using GPS," in *Proc. AVEC Int. Symp. Adv. Veh. Control*, 2002, pp. 373–380.
[21] H. K. Khalil, "Feedback linearization," in *Nonlinear Systems*, 3rd ed. Hoboken, NJ, USA: Prentice Hall, 2002, pp. 505–550.
[22] M. Nagai, M. Shino, and F. Gao, "Study on integrated control of active front steer angle and direct yaw moment," *JSAE Rev.*, vol. 23, no. 3, pp. 309–315, 2002.
[23] M. A. Henson and D. E. Seborg, "Feedback linearizing control," in *Nonlinear Process Control*, vol. 4. Hoboken, NJ, USA: Prentice Hall, 1997, pp. 149–231.
[24] G. Phanomchoeng and R. Rajamani, "Real-time estimation of rollover index for tripped rollovers with a novel unknown input nonlinear observer," *IEEE/Amer. Soc. Mech. Engineers Trans. Mechatronics*, vol. 19, no. 2, pp. 743–754, Apr. 2014.
[25] C. Larish, D. Piyabongkarn, V. Tsourapas, and R. Rajesh, "A new predictive lateral load transfer ratio for rollover prevention systems," *IEEE Trans. Veh. Technol.*, vol. 62, no. 7, pp. 2928–2936, Sep. 2013.
[26] Y. Furukawa, N. Yuhara, S. Sano, H. Takeda, and Y. Matsushita, "A review of four-wheel steering studies from the viewpoint of vehicle dynamics and control," *Veh. Syst. Dyn.*, vol. 18, pp. 151–186, 1989.
[27] Y. Huang and Y. Chen, "Estimation and analysis of vehicle lateral stability region with both front and rear wheel steering," in *Proc. ASME Dyn. Syst. Control Conf.*, 2017, Paper DSCC20175154.

Fengchen Wang (Member, IEEE) received the B.S. and M.S. degrees (with Hons.) in automotive engineering from China Agricultural University, Beijing, China, in 2014 and 2016, respectively, and the Ph.D. degree in systems engineering from Arizona State University, Mesa, AZ, USA, in 2020. He is currently working toward the second M.S. degree in computer science with the Georgia Institute of Technology, Atlanta, GA, USA. He is the author or co-author of more than 25 peer-reviewed publications. His research interests include control theory and application, vehicle dynamics and control, connected and automated vehicle technology, and complex network system modeling, analysis, control, and optimization.

Yue Shi received the B.S. and Ph.D. degrees in mechanical engineering from Shanghai Jiao Tong University, Shanghai, China, in 2009 and 2018, respectively. From 2018 to 2019, he was with Polytechnic School, Arizona State University, Mesa, AZ, USA, as a Postdoctoral Research Associate. His research interests include vehicle system dynamics and control, active safety system design, trajectory planning, and rollover prevention for autonomous trucks.

Yan Chen (Member, IEEE) received the B.S. and M.S. degrees (with Hons.) in control science and engineering from the Harbin Institute of Technology, Harbin, China, in 2004 and 2006, respectively, the second M.S. degree in mechanical engineering from Rice University, Houston, TX, USA, in 2009, and the Ph.D. degree in mechanical engineering from Ohio State University, Columbus, OH, USA, in 2013. He is currently an Assistant Professor with Arizona State University, Mesa, AZ, USA. He is the author or co-author of more than 75 peer-reviewed publications. His research interests include design, modeling, estimation, control, and optimization of dynamic systems, specifically for automated and connected ground vehicle, electric vehicle, internal combustion engine, powertrain, aftertreatment, multiagent, and mechatronic systems. He is an Associate Editor for the journals of IEEE TRANSACTIONS ON VEHICULAR TECHNOLOGY and *IFAC Mechatronics*. He is the Chair of ASME Automotive and Transportation Systems Technical Committee.